ISIJ International, Vol. 53 (2013), No. 8, pp. 1334–1340

In situ X-ray Diffraction Investigation of the Formation Mechanisms of Silico-Ferrite of Calcium and Aluminium-I-type (SFCA-I-type) Complex Calcium Ferrites

Nathan A. S. WEBSTER,[1,2)]* Mark I. POWNCEBY[1)] and Ian C. MADSEN[1)]

1) CSIRO Process Science and Engineering, Box 312, Clayton South, VIC, 3169 Australia.
2) Australian Nuclear Science and Technology Organisation, Locked Bag 2001, Kirrawee DC, NSW, 2232 Australia.

(*Received on March 18, 2013; accepted on May 15, 2013*)

The formation mechanisms of the complex Ca-rich ferrite phase SFCA-I, an important bonding material in iron ore sinter, during heating of synthetic sinter mixtures in the temperature range 298–1 623 K in air and at $pO_2 = 5 \times 10^{-3}$ atm, were determined using *in situ* X-ray powder diffraction. In air, the initial formation of SFCA-I at ~1 438 K (depending on composition) was associated with reaction of precursor phases Fe_2O_3, $CaO{\cdot}Fe_2O_3$, SiO_2, amorphous Al-oxide and a CFA phase of approximate composition 71.7 mass% Fe_2O_3, 12.9 mass% CaO, 0.3 mass% SiO_2 and 15.1 mass% Al_2O_3. At temperatures above ~1 453 K, the decomposition of another phase, γ-CFF, resulted in the formation of additional SFCA-I. At lower oxygen partial pressure the initial formation of SFCA-I occurred at similar temperatures and was associated with reaction between similar phases as its formation in air. However, the decomposition of γ-CFF did not result in the formation of additional SFCA-I, with the maximum SFCA-I concentration (25 mass%) lower than the values attained in air (54 and 34 mass%). Hence, more oxidising conditions appear to favour the formation of the desirable SFCA-I phase.

KEY WORDS: iron ore sinter; SFCA and SFCA-I; *in situ* X-ray diffraction; Rietveld refinement-based quantitative phase analysis; SFCA-I formation mechanisms.

1. Introduction

A number of investigations[1–10)] have aimed to determine the formation mechanisms of 'SFCA' (Silico-Ferrite of Calcium and Aluminium) complex Ca-rich ferrite iron ore sinter bonding phases. SFCA phases are key components of industrial iron ore sinter, and increased understanding of their formation mechanisms has the potential to improve the efficiency of the sintering process by i) being able to predict the optimal sintering conditions (*e.g.* temperature, oxygen partial pressure) to produce high-quality product based on the chemical composition and physical characteristics of a given starting iron ore sinter mixture, and ii) being able to predict the chemical and physical modifications of a particular starting iron ore sinter mixture that are required to produce high-quality product.

The 'SFCA' produced in iron ore sinter has, in the past, been categorised on the basis of composition, structure and morphology into two main types. The first is a high-Fe, low-Si form called SFCA-I which has a characteristic platy (also described as acicular or needle-like) morphology. Mumme *et al.*[11)] reported that an SFCA-I phase found in industrial plant sinter contained 84 mass% Fe_2O_3, 13 mass% CaO, 1 mass% SiO_2 and 2 mass% Al_2O_3, and successfully synthesised material with the SFCA-I structure which had the composition 83.2 mass% Fe_2O_3, 12.6 mass% CaO and 4.2 mass% Al_2O_3. The SFCA-I crystal structure (space group = $P\bar{1}$, a = 10.43, b = 10.61, c = 11.84 Å, α = 94.14, β = 111.35, γ = 110.27°) was determined from a crystal with the latter composition. McAndrew and Clout[12)] suggested that a texture of intersecting microplates characteristic of SFCA-I imparts high strength and reducibility into iron ore sinter, and sinters containing significant amounts of this phase are considered to be of high quality.

The second 'SFCA' type is a low-Fe form that is simply referred to as SFCA, and which exhibits a prismatic or columnar morphology. SFCA found in industrial plant sinters typically contains 60–76 mass% Fe_2O_3, 13–16 mass% CaO, 3–10 mass% SiO_2, 4–10 mass% Al_2O_3 and 0.7–1.5 mass% MgO.[13,14)] Patrick and Pownceby[15)] systematically resolved the equilibrium solid solution range and thermal stability of SFCA within the quaternary system Fe_2O_3–CaO–SiO_2–Al_2O_3 in air at 1 513–1 663 K. Such a rigorous investigation of solid solution limits and thermal stability has not been performed for SFCA-I. However, based on the work of Mumme *et al.*,[11)] it is expected that the solid solution range would be narrower in comparison with SFCA.

In one of the most recent of the mechanistic investigations, Webster *et al.*[9)] implemented *in situ* X-ray diffraction (XRD) in order to characterise the reaction sequences in the formation of SFCA phases from synthetic starting mixtures

* Corresponding author: E-mail: nathan.webster@csiro.au
DOI: http://dx.doi.org/10.2355/isijinternational.53.1334

in the temperature range 298–1 623 K and at an oxygen partial pressure (pO_2) of 5×10^{-3} atm. The selection of the pO_2 was based on the work of Hsieh and Whiteman,[2] where it was shown that a pO_2 of 5×10^{-3} atm maximised the formation of Ca-rich ferrite phases, whilst producing mineral assemblages similar to those found in industrial sinters. It was shown by Webster *et al.*[9] that during heating, SFCA-I formation at ~1 373 K was associated with reaction between Fe_2O_3, SiO_2 and Al_2O_3-substituted dicalcium ferrite [designated $C_2(F_{1-x}A_x)$]. In comparison, SFCA formation occurred at ~1 433 K and was associated with reaction between calcium ferrite (*i.e.* $CaO{\cdot}Fe_2O_3$, designated CF), SiO_2, and a phase designated CFA which had average composition 71.7 mass% Fe_2O_3, 12.9 mass% CaO, 0.3 mass% SiO_2 and 15.1 mass% Al_2O_3. Whilst the initial formation of SFCA was determined to be independent of SFCA-I, at higher temperatures the breakdown of SFCA-I was associated with formation of additional SFCA. Equations (1) and (2) (unbalanced) summarise the reactions involved in the formation of SFCA-I and SFCA determined by Webster *et al.*[9] (the '±' in Eq. (2) represents the initial formation of SFCA being independent of SFCA-I).

$$Fe_2O_3 + C_2(F_{1-x}A_x) + SiO_2 \rightarrow \text{SFCA-I} \quad \text{..... (1)}$$

$$CF + CFA + Fe_2O_3 + SiO_2 + \text{Al-oxide} \pm \text{SFCA-I} \rightarrow \text{SFCA} \quad \text{..... (2)}$$

In a follow-up investigation, Webster *et al.*[10] used similar methodology to determine the effect of oxygen partial pressure, in the range 0.21 to 1×10^{-4} atm, on the formation mechanisms of the SFCA phases. In air, SFCA-I and SFCA formed according to the mechanisms summarised in Eqs. (3) and (4).

$$Fe_2O_3 + CF + SiO_2 + CFA + \text{Al-oxide} \rightarrow \text{SFCA-I} \quad \text{..... (3)}$$

$$Fe_2O_3 + CF + SiO_2 + \text{Al-oxide} \pm \text{SFCA-I} \rightarrow \text{SFCA} \quad \text{.... (4)}$$

At the more reduced oxygen partial pressure of $pO_2 = 1 \times 10^{-4}$ atm, however, SFCA-I did not form. Instead, a Ca-rich phase designated CF_{AlSi} and having a composition of 71.6 mass% Fe_2O_3, 24.1 mass% CaO, 0.3 mass% SiO_2 and 2.4 mass% Al_2O_3 formed at ~1 423 K. By ~1 453 K this phase had decomposed to form melt and a small amount of SFCA. Equations (5) and (6) summarise the formation mechanisms at $pO_2 = 1 \times 10^{-4}$ atm (Fe_3O_4 = magnetite).

$$C_2(F_{1-x}A_x) + CF + SiO_2 + Fe_3O_4 \rightarrow CF_{AlSi} \quad \text{..... (5)}$$

$$CF_{AlSi} \rightarrow \text{SFCA} + \text{melt} \quad \text{..... (6)}$$

In both of the Webster *et al.*[9,10] studies, and also in the earlier *in situ* XRD studies of Scarlett *et al.*,[7,8] the starting sinter mixture compositions were all located within the SFCA composition domain established by Patrick and Pownceby.[15] Subsequently, it was hypothesised that by altering the composition of the starting sinter mixtures to those established by Mumme *et al.*[11] to be within the SFCA-I compositional domain, the reaction mechanisms may be altered. The current investigation was designed to test this hypothesis, through a series of *in situ* XRD and heat/quench experiments under both oxidizing (pO_2 = 0.21 atm) and more reducing ($pO_2 = 5 \times 10^{-3}$ atm) conditions, in order to characterize the phase evolution in sinter mixtures specifically designed to form the more desirable SFCA-I phase.

2. Experimental

2.1. Starting Sinter Mixture Preparation

The starting sinter mixtures had compositions of 83.2 mass% Fe_2O_3, 12.6 mass% CaO and 4.2 mass% Al_2O_3 (designated SFCA-I-a); and 84 mass% Fe_2O_3, 13 mass% CaO, 1 mass% SiO_2 and 2 mass% Al_2O_3 (SFCA-I-b). They were prepared from fine grained (< 20 μm) synthetic hematite, Fe_2O_3 (Acros Organics, 99.999%), calcite, $CaCO_3$ (Thermo Fisher, 99.95%), quartz, SiO_2 (Sigma Aldrich, 99.995), and gibbsite, $Al(OH)_3$ (Alcan OP25 Super White, 99.9%). These were mixed under acetone in a mortar and pestle to ensure homogeneity.

2.2. *In Situ* XRD

In situ XRD experiments were performed using an INEL diffractometer, which incorporates a CPS120 position-sensitive detector allowing for simultaneous collection of up to 120° 2θ of diffraction data. The Co X-ray tube was operated at 40 kV and 35 mA. An Anton Paar model HTK 10 high temperature chamber, employing a platinum resistance strip heater, was positioned on the instrument. A slurry of the sinter sample mixture and ethanol was prepared and placed into the sample well, measuring approximately $20 \times 7 \times 0.2$ mm deep, on the platinum heater. Three *in situ* experiments were performed: one for each of the SFCA-I-a and SFCA-I-b mixtures in air, referred to hereafter as "SFCA-I-a-air" and "SFCA-I-b-air"; and one for the SFCA-I-b mixture at $pO_2 = 5 \times 10^{-3}$ atm (*i.e.* "SFCA-I-b-0.005"). Compressed air, and a gas cylinder containing 0.5% O_2 in N_2 (Coregas), were used to achieve the desired atmospheres. The Anton Paar chamber was purged for 30 min by a flow (~1 L min^{-1}) of the designated gas, after which the sample was heated under a continuous flow of the gas.

A heating rate of 20 K min^{-1} was used from 298 to 873 K (approaching the decomposition temperature of $CaCO_3$), then a rate of 10 K min^{-1} to 1 623 K was used during the period of SFCA-I phase formation and melting. The temperature was measured by a Pt/PtRh10% thermocouple connected to the underside of the platinum strip. *In situ* XRD data were collected throughout heating, with individual datasets collected for 0.5 min. Data were collected in asymmetrical diffraction geometry with a fixed incident beam angle of 10°, over the range $10° \leq 2\theta \leq 112°$. Temperatures were automatically recorded at the start of each dataset. Where absolute temperature values are quoted throughout the remainder of the manuscript, the uncertainty in these values was the difference between the temperatures at the start of successive datasets. The magnitude of the uncertainty, therefore, varied according to the heating rate and was ~10 and 5 K for the 20 and 10 K min^{-1} heating regimes, respectively.

2.3. *In Situ* XRD Data Analysis

The decomposition of precursor phases and the formation of new phases as the experiments progressed was visualised by stacking the datasets to produce plots of accumulated data with temperature plotted *vs* 2θ, viewed down the intensity axis. For the purpose of extracting phase abundances as a function of temperature, Rietveld refinement-based quantitative phase analysis (QPA) was performed using TOPAS.[16] The crystal structure information provided in Blake *et al.*,[17]

Maslen *et al.*,[18] Saalfeld and Wedde,[19] Lager *et al.*,[20] Oftedal,[21] Bersetegui *et al.*,[22] Decker and Kasper,[23] Arakcheeva and Karpinskii,[24] Mumme *et al.*[11] and Hamilton[25] was used for Fe_2O_3, $CaCO_3$, $Al(OH)_3$, SiO_2, CaO, $C_2(F_{1-x}A_x)$, CF, γ-CFF, SFCA-I and Fe_3O_4, respectively. Corrections to account for sample displacement errors and to scale peak intensities in the asymmetrical diffraction geometry were incorporated into the TOPAS refinement algorithm.[26]

The use of the Hill & Howard[27] QPA algorithm embodied in TOPAS returns *relative*, rather than *absolute*, concentrations for crystalline phases in a system if amorphous material, including melt phases, are present. In order to determine the absolute phase concentrations (in mass%) as a function of temperature, the 'external standard' approach[28] embodied in Eq. (7) was used:

$$W_i = \frac{\mu_m^* S_i (ZMV)_i}{K} \quad \text{..... (7)}$$

Here, W_i is the mass% of phase i, S_i is the Rietveld scale factor, ZM is the unit-cell mass, V is the unit-cell volume, μ_m^* is the mass absorption coefficient of the entire mixture, and K is a scaling factor used to put W_i on an absolute basis. K is constant in an experiment as long as the experimental conditions do not change, and was calculated using i) the known concentrations of Fe_2O_3, $CaCO_3$, SiO_2 and $Al(OH)_3$ in the starting mixture, and ii) the Rietveld-refined scale factors for Fe_2O_3, $CaCO_3$, SiO_2 and $Al(OH)_3$ in the first dataset collected at 25°C, using Eq. (8).

$$K = \frac{\mu_m^* \sum_{i=1}^{n} S_i (ZMV)_i}{\sum_{i=1}^{n} W_i} \quad \text{..... (8)}$$

2.4. Heat/Quench Experiments and *Ex Situ* Characterisation

Laboratory heat/quench experiments were performed to investigate in more detail the key phases revealed by the *in situ* XRD experiments. For these experiments, 0.5 g of the starting sinter mixture was pelletised and heated at temperature for 3 hr in a platinum crucible in a vertical tube furnace under the required atmosphere. The temperature adjacent to the crucible was measured using a Pt/PtRh13% thermocouple connected to an ice-point cell, and temperatures are considered accurate to ± 10 K. Samples were rapidly quenched by dropping the crucible to the cold end of the furnace; the furnace atmosphere (air or $pO_2 = 5 \times 10^{-3}$ atm) was constant throughout the quench procedure. Samples were crushed and a small piece was collected and prepared for *ex situ* scanning electron microscopy (SEM), energy dispersive spectroscopy (EDS) and electron probe microanalysis (EPMA).

SEM was performed using a FEI Quanta 400 Field Emission Environmental Scanning Electron Microscope operated at an accelerating voltage of 15 kV and a working distance of 10 mm. EDS was performed using a Bruker X-Flash 5010 Si-drift EDS detector. EPMA was performed using a JEOL JXA-8900F Superprobe. Fe_2O_3, wollastonite ($CaSiO_3$, CS) and "Magalox" (a synthetic spinel, composition $MgAl_2O_4$) were used as standards for the microprobe analyses which were conducted in wavelength dispersive mode using an accelerating voltage of 12 kV, a beam diameter of < 1 μm and counting times of 15 sec on the peak (7.5 sec on the background).

3. Results and Discussion

3.1. Phase Evolution

Figures 1(a), 1(b), and 1(c) show plots of accumulated *in*

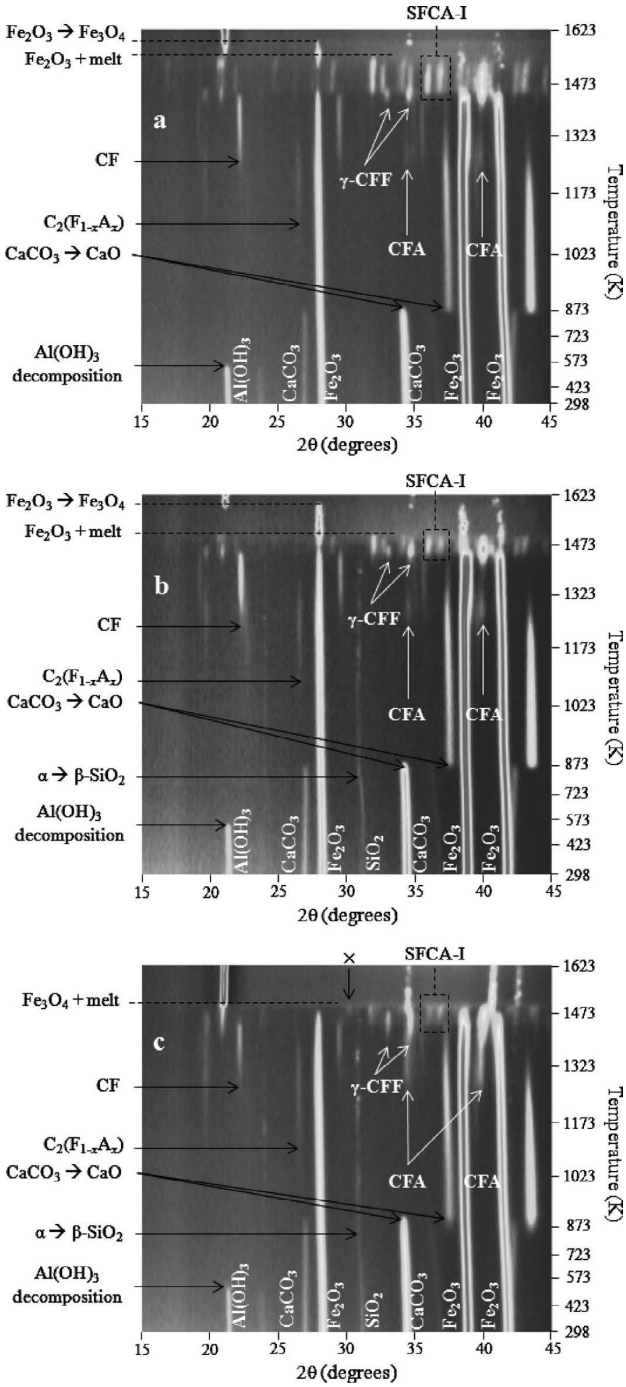

Fig. 1. *In situ* XRD data collected for a) SFCA-I-a-air, b) SFCA-I-b-air and c) SFCA-I-b-0.005. Annotated on the plots are: the major reflections for materials in the starting mixture; the low-temperature (< 923 K) phase transformation (*e.g.* $\alpha \rightarrow \beta$-SiO_2) and decomposition (*e.g.* $CaCO_3 \rightarrow CaO$) events; the formation events of $C_2(F_{1-x}A_x)$, CF, γ-CFF, SFCA-I, and the Fe_2O_3/Fe_3O_4 + melt phase assemblage; and the major reflections for CFA. For (c), '×' denotes the reflection for the unknown phase. (Online version in colour).

situ XRD data for the experiments SFCA-I-a-air, SFCA-I-b-air and SFCA-I-b-0.005, respectively. The low-temperature (<1 123 K) phase decomposition and transformation events in each case are very similar to those reported previously by Webster *et al.*[9,10] and are discussed only briefly here. In each experiment $Al(OH)_3$ decomposed to amorphous Al-oxide and the decomposition was complete by ~553 K. For the SFCA-I-b-air experiment, where the starting sinter mixture contained 1 mass% SiO_2, the transformation of α-SiO_2 to β-SiO_2 occurred at 839 K which is in good agreement with the 846 K reported by Kihara[29] and gives confidence in the accuracy of the temperature measurement. In each experiment decomposition of $CaCO_3$ to CaO was complete by ~898 K. The first Ca-rich ferrite to form was $C_2(F_{1-x}A_x)$ at ~1 053 K, followed by CF and CFA together at ~1 233 K.

For each of the SFCA-I-a-air, SFCA-I-b-air and SFCA-I-b-0.005 experiments the next phase to form, at 1 396, 1 405 and 1 384 K, respectively, was one which was isostructural with the γ-CFF phase reported by Arakcheeva and Karpinskii,[24] ($Ca_{3.0}Fe_{14.82}O_{25}$; ICDD entry no. 1-078-1675; hexagonal unit cell, a = 5.985, c = 15.748 Å). Mumme *et al.*[11] previously showed the location of this phase within phase diagrams for the Fe_2O_3/Al_2O_3–CaO–FeO and Fe_2O_3/Al_2O_3–CaO–SiO_2 systems. The formation of γ-CFF is a significant difference between the present results and those described previously by Webster *et al.*[9,10] and Scarlett *et al.*[7,8] for mixtures with compositions designed to form SFCA and for which the reaction mechanisms given by Eqs. (1)–(4) applied.

In each experiment the next phase to form was SFCA-I. For the SFCA-I-a-air experiment SFCA-I was first observed at 1 442 K, and was present until it melted to form a Fe_2O_3 + melt phase assemblage at 1 554 K. As the temperature increased further the Fe_2O_3 transformed to Fe_3O_4 producing a Fe_3O_4 + melt phase assemblage. The spotty nature of some of the Fe_2O_3 and Fe_3O_4 reflections at T > 1 498 K is caused by poor particle statistics and, most likely, preferred orientation of the relatively small number of crystallites dispersed in a larger amount of melt. Hence, QPA was not performed for temperatures above 1 573 K. It is possible that translating the sample stage back and forth in the sample plane would alleviate these effects, but that was not possible on this instrument. Similar phases and phase assemblages were observed for the SFCA-I-b-air experiment, but with a narrower thermal stability range of SFCA-I before melting (1 433–1 514 K). The lower melting point for the SFCA-I-b sample, which has the lower Al_2O_3 concentration, is consistent with the results of Webster *et al.*[9]

The reduction of Fe_2O_3 to Fe_3O_4 at T = 1 594 K and T = 1 603 K for SFCA-I-a-air and SFCA-I-b-air, respectively, is a further difference between this experiment and the experiment conducted in air by Webster *et al.*,[10] where Fe_2O_3 remained the stable phase up to 1 623 K. Since SFCA was not observed to form in the SFCA-I-a-air and SFCA-I-b-air *in situ* experiments, it is suggested that these mixtures result in an increased concentration of Ca^{2+} in the melt after decomposition of SFCA-I which would otherwise be incorporated into the SFCA structure in a mixture designed to form SFCA. Subsequent reaction between the Ca-rich melt and Fe_2O_3 increases the activity of Ca^{2+} in Fe_2O_3 and lowers the temperature of the Fe_2O_3 to Fe_3O_4 reduction reaction[30] from the theoretical value in air of 1 682 K.[31]

For the SFCA-I-b-0.005 experiment (Fig. 1(c)), SFCA-I formed at 1 444 K and was stable until the incongruent melting of SFCA-I was complete by 1 509 K, forming the assemblage Fe_3O_4 + melt. The formation of Fe_3O_4 by incongruent melting (of SFCA) was also observed by Webster *et al.*[9] for experiments conducted at $pO_2 = 5 \times 10^{-3}$ atm.

Figures 2(a) and 2(b) show backscattered electron micrographs of the product of a heat/quench experiment performed for the SFCA-I-b mixture at 1 453 K for 3 hr at $pO_2 = 5 \times 10^{-3}$ atm. Note that Figs. 2(a) and 2(b) show an identical region of the sample, with the contrast and brightness settings of the electron microscope optimised in Fig. 2(a) to distinguish the compositionally similar phases SFCA-I and γ-CFF. This resulted in the region of amorphous Al-oxide having the same very dark contrast as pores, which are clearly distinguishable in Fig. 2(b). EDS analysis confirmed the presence of Si in the regions designated as SFCA-I, and the absence of Si in the regions designated as γ-CFF. Compositional results for the phases shown in Fig, 2(a) (and for CF which is not present in Fig. 2(a) but was observed in other regions of the sample) obtained via EPMA are summarised in **Table 1**. Figure 2(a) also shows that SFCA-I surrounded regions of CFA, with CFA encapsulating grains of Al-oxide. γ-CFF was typically found in direct contact with the SFCA-I.

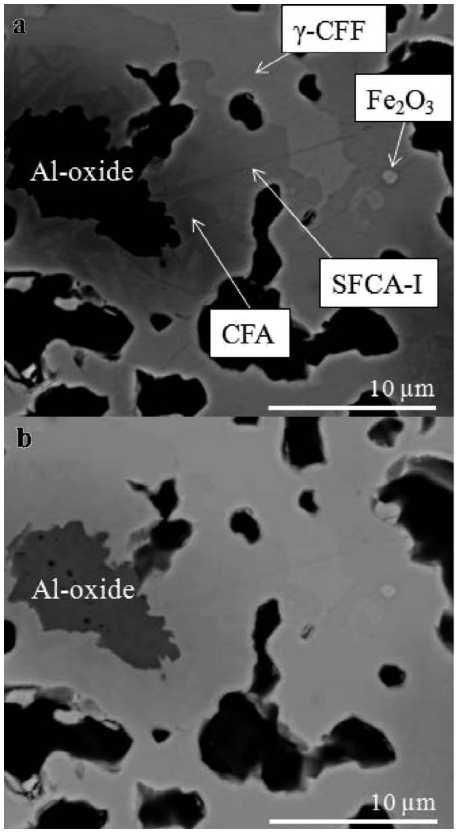

Fig. 2. a) Backscattered electron micrograph of the product of the heat/quench experiment performed for the mixture SFCA-I-b at 1 453 K for 3 hr at $pO_2 = 5 \times 10^{-3}$ atm. Annotated are regions of SFCA-I, γ-CFF, CFA, Fe_2O_3, and Al-oxide, and b) the same field of view but at different contrast and brightness to distinguish Al-oxide from the pores (black areas in image).

Table 1. Summary of the EPMA compositional results, in terms of mass% oxides, for the product of the heat/quench experiment performed for SFCA-I-b at 1 453 K for 3 hr at $pO_2 = 5 \times 10^{-3}$ atm. The numbers in parentheses are the standard deviations of 5 point analyses for each phase.

Phase	Composition (mass%)				
	Fe_2O_3	CaO	SiO_2	Al_2O_3	Total
SFCA-I	82.82 (0.66)	13.70 (0.12)	0.19 (0.05)	1.67 (0.53)	98.38 (0.30)
γ-CFF	85.01 (0.54)	12.34 (0.10)	0.02 (0.01)	0.62 (0.05)	97.99 (0.55)
CFA	69.28 (5.23)	12.41 (0.52)	0.12 (0.15)	14.87 (5.59)	96.68 (0.37)
Fe_2O_3	97.63 (0.24)	0.55 (0.21)	0.01 (0.01)	0.23 (0.03)	98.41 (0.11)
CF	73.11 (0.27)	25.22 (0.16)	0.01 (0.01)	0.16 (0.02)	98.49 (0.17)

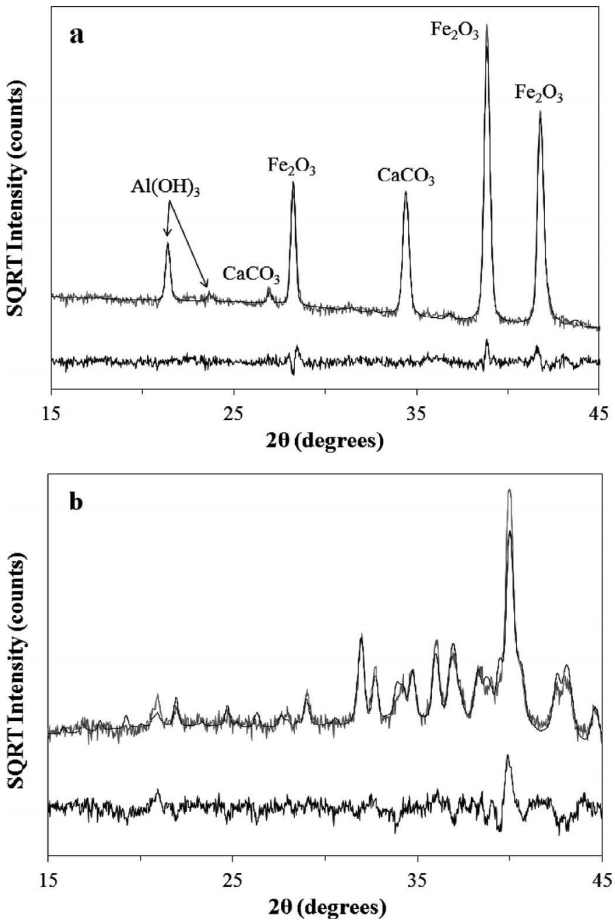

Fig. 3. Rietveld fit for the dataset collected at a) 298 K, and b) 1 488 K, during the *in situ* XRD experiment SFCA-I-a-air. Experimental data are shown as scattered solid lines, the calculated patterns as smooth solid lines and the difference pattern as solid lines below. Reflections for Fe_2O_3, $CaCO_3$ and $Al(OH)_3$ are annotated in (a). (Online version in colour).

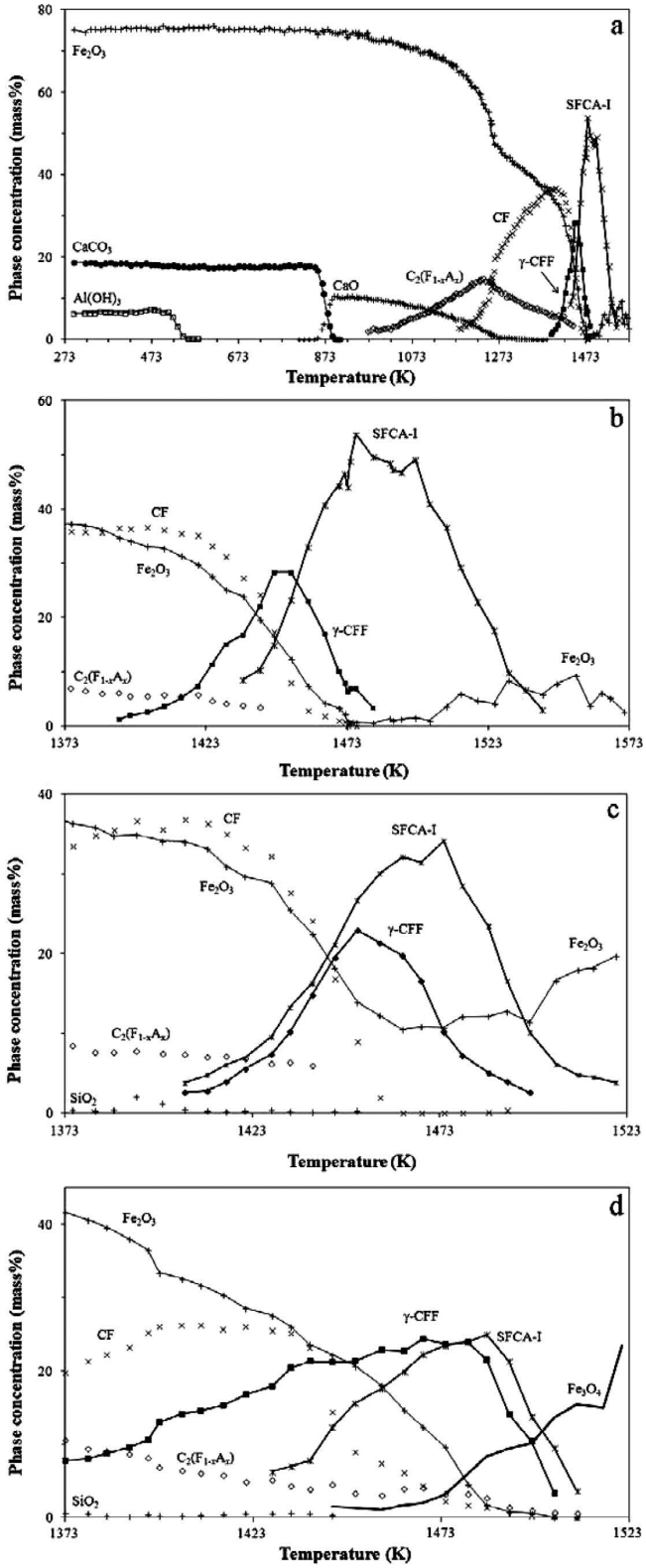

Fig. 4. Results of the QPA, derived using the relationship shown in Eq. (7), showing absolute phase abundances as a function of temperature for the a) SFCA-I-a-air, b) SFCA-I-a-air over the range 1 373–1 573 K, c) SFCA-I-b-air and d) SFCA-I-b-0.005, *in situ* XRD experiments.

3.2. QPA and Reaction Mechanisms in Air

Figures 3(a) and 3(b) show the Rietveld fits for the datasets collected at 298 and 1 488 K (*i.e.* where SFCA-I was the only phase present) during the SFCA-I-a-air experiment, respectively. The quality of the fit (χ^2 = 1.61 and 1.72, respectively) was similar for each dataset. **Figure 4**(a) shows the results of the Rietveld refinement-based QPA for the SFCA-I-a-air experiment, and includes the low-temperature region where decomposition of $Al(OH)_3$ to amorphous Al-oxide material was observed, as well as the formation of CaO through decomposition of $CaCO_3$, the reaction of Fe_2O_3 and CaO to form $C_2(F_{1-x}A_x)$, and reaction of Fe_2O_3 and $C_2(F_{1-x}A_x)$ to form CF. Figure 4(b) displays only the high-temperature region (>1 373 K) for this experiment, and more clearly shows the concentration curves for γ-CFF and

SFCA-I. Figures 4(c) and 4(d) display similar high-temperature regions for the SFCA-I-b-air and SFCA-I-b-0.005 experiments, respectively. In the absence of any previously published structural information for CFA necessary to perform Rietveld refinement-based QPA of this phase, QPA of CFA could not be included in Figs. 4(a)–4(d).

In Figs. 4(a) and 4(b) the formation of γ-CFF was associated with reaction between Fe_2O_3 and CF. Given that the concentrations of Fe_2O_3 and CF decreased at a similar rate during this regime, this raises the question as to why γ-CFF and not CF_2 (*i.e.* $CaO{\cdot}2Fe_2O_3$) was observed. The answer appears to lie in the Fe_2O_3/Al_2O_3–CaO–FeO phase diagram presented by Mumme *et al.*[11] and reproduced here in **Fig. 5**; the formation of γ-CFF implies the presence of Fe^{2+} in the system even under these oxidising conditions. The presence of Fe^{2+} in SFCA-I material synthesised in air has been described recently by Webster *et al.*,[10] with the SFCA-I composition located in close proximity to γ-CFF in Fig. 5.

The initial formation of SFCA-I was also associated with a decrease in the concentration of CF and Fe_2O_3, and these phases were fully consumed by 1 473 K. After the concentration of γ-CFF reached a maximum of 29 mass% at 1 447 K, the decomposition of γ-CFF resulted in the formation of additional SFCA-I. The SFCA-I concentration reached a maximum of 50 mass% at 1 473 K, before it melted incongruently to form an Fe_2O_3 + melt phase assemblage, with a small increase in the Fe_2O_3 concentration evident in Figs. 4(a) and 4(b) during melting of SFCA-I.

For the SFCA-I-b-air experiment shown in Fig. 4(c), the formation of γ-CFF and SFCA-I was associated with the reaction of similar phases as for the SFCA-I-a-air experiment. Also, incongruent melting of SFCA-I above 1 473 K was associated with an increase in Fe_2O_3 concentration. Notable differences from the SFCA-I-a-air experiment include i) the decay of the SiO_2 concentration to 0 mass% in the early stages of SFCA-I formation; the negligible Si content of the γ-CFF phase in the product of the heat/quench experiment (see Fig. 2(a) and Table 1) provides additional evidence that SiO_2 is consumed in the formation of SFCA-I only; ii) the incomplete consumption of Fe_2O_3, with 10 mass% of unreacted Fe_2O_3 still present when CF is fully consumed; and iii) the lower maximum SFCA-I concentration of 34 mass%. Following on from the latter observation, a starting sinter mixture with composition closer to that of SFCA-I-a compared to SFCA-I-b (*i.e.* with a low SiO_2 content and higher Al_2O_3 content), should maximise the formation of the SFCA-I phase desirable for high quality iron ore sinter.

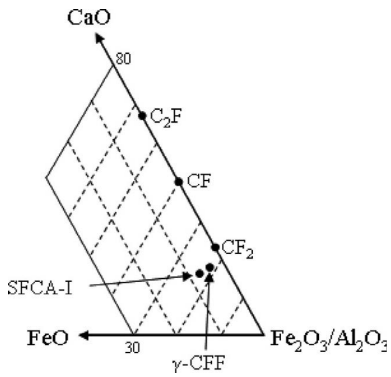

Fig. 5. Part of the Fe_2O_3/Al_2O_3–CaO–FeO system showing the location of CF_2, γ-CFF and SFCA-I (after Mumme *et al.*).[11] The unit of each axis is mass%.

Because of the amorphous nature of the Al-oxide which formed after decomposition of $Al(OH)_3$ at 533 K, and the inability to include CFA in the QPA for the reason described earlier, it is not possible to directly observe the fate of these phases in Figs. 4(a)–4(d). However, SEM micrographs for the product of a heat/quench experiment performed for the SFCA-I-a sample at 1 453 K in air for 3 hr showed that, similarly to the micrograph shown in Fig. 2(a), SFCA-I was in contact with the regions of CFA. CFA, and the Al-oxide encapsulated by the CFA phase, therefore, is most likely involved in the reaction to form SFCA-I. Equations (9) and (10) summarise the formation mechanisms of γ-CFF and SFCA-I in air:

$$Fe_2O_3 + CF \rightarrow \gamma\text{-CFF} \quad \text{.....} (9)$$

$$Fe_2O_3 + CF + SiO_2\,(\text{if present}) + CFA + \text{Al-oxide} \pm \gamma\text{-CFF} \rightarrow \text{SFCA-I} \quad \text{.....} (10)$$

3.3. QPA and Reaction Mechanisms, $pO_2 = 5 \times 10^{-3}$ Atm

The mechanism of γ-CFF formation (at 1 384 K) in the SFCA-I-b-0.005 experiment (Fig. 4(d)) differed from that in air, with its formation associated with reaction between Fe_2O_3 and $C_2(F_{1-x}A_x)$. The different mechanism is attributed to the earlier onset of γ-CFF formation, in this case being within the temperature regime where CF was still being formed; in Fig. 4(d) the CF concentration increased by a small amount between 1 384 and 1 395 K, before plateauing at ~25 mass% in the range 1 395–1 433 K. A decrease in the CF concentration at 1 438 K coincided with the formation of SFCA-I, and was also associated with a further reduction in the Fe_2O_3 concentration. In contrast to the SFCA-I-a-air and SFCA-I-b-air experiments, decomposition of γ-CFF above 1 473 K did not result in the formation of a significant amount of additional SFCA-I. Re-examination of the *in situ* XRD data shown in Fig. 1(c) revealed that, upon decomposition of γ-CFF, the formation of an additional, unknown phase (indicated by the reflection annotated with '×' in Fig. 1(c), which was not apparent in Figs. 1(a) and 1(b)) occurred instead. SFCA-I reached a maximum concentration of only 25 mass% before melting to form the Fe_3O_4 + melt phase assemblage. An oxidising environment, therefore, appears favourable to maximise the formation of the desirable SFCA-I phase. Similarly to the experiments conducted in air, CFA and Al-oxide are most likely involved in the reaction to form SFCA-I, and Eqs. (11) and (12) summarise the formation mechanism of γ-CFF and SFCA-I at $pO_2 = 5 \times 10^{-3}$ atm:

$$Fe_2O_3 + C_2(F_{1-x}A_x) \rightarrow \gamma\text{-CFF} \quad \text{.....}(11)$$

$$Fe_2O_3 + CF + SiO_2\,(\text{if present}) + CFA + \text{Al-oxide} \rightarrow \text{SFCA-I} \quad \text{.....} (12)$$

Based on a comparison of Eqs. (11) and (12) with Eqs. (1) and (2) (*i.e.* the reaction mechanisms for SFCA-I and SFCA, respectively, at $pO_2 = 5 \times 10^{-3}$ atm given in Section 1), the more Fe-rich γ-CFF and SFCA-I phases replace SFCA-I and SFCA, respectively, in the reaction sequences

when the starting sinter mixture is designed to form SFCA-I. The similarity between the temperatures of formation of γ-CFF (1 384 K) and SFCA-I (1 444 K) determined here, with those determined by Webster *et al.*[9] for SFCA-I and SFCA (1 392 and 1 437 K, respectively), provides further evidence for this. The γ-CFF phase, therefore, appears to have comparable significance to SFCA-I and SFCA in the context of complex calcium ferrite iron ore sinter bonding phases. It is unknown what effects γ-CFF would have on the physical properties of a sinter product, and it is considered worthwhile to conduct a systematic investigation of the strength, reducibility and reduction degradation properties of pure samples of each of the phases SFCA-I, SFCA and γ-CFF, in order to ascertain what the effects may be. Future work will also involve determination of the unknown phase formed upon decomposition of γ-CFF in the *in situ* XRD experiment performed at $pO_2 = 5 \times 10^{-3}$ atm.

4. Conclusion

The formation of SFCA-I and precursor phases during heating of synthetic sinter mixtures designed to form SFCA-I in the range 298–1 623 K in air and at $pO_2 = 5 \times 10^{-3}$ atm, were characterised using an *in situ* X-ray diffraction-based methodology. Under both atmospheres the formation of SFCA-I at ~1 438 K (depending on composition) was preceded by the formation of a γ-CFF phase. In air γ-CFF formation was associated with reaction of Fe_2O_3 and CF, and at $pO_2 = 5 \times 10^{-3}$ atm through reaction of Fe_2O_3 and $C_2(F_{1-x}A_x)$. Under both atmospheres the initial formation of SFCA-I was associated with reaction of Fe_2O_3, CF, SiO_2 (if present), CFA and amorphous Al-oxide, the main difference being that in air the decomposition of γ-CFF at >1 453 K resulted in the formation of additional SFCA-I which was not the case at the lower oxygen partial pressure. These experiments have shown that in order to maximise the concentration of the desirable SFCA-I phase in iron ore sinter, oxidising conditions and a mixture low in SiO_2 and higher in Al_2O_3 are required.

Acknowledgements

The Australian Nuclear Science and Technology Organisation (ANSTO) are acknowledged for their financial support of this research. The authors wish to thank: Matthew Glenn (CSIRO Process Science and Engineering) for assistance with SEM; Nick Wilson (CSIRO Process Science and Engineering) for assistance with EPMA, and Cameron Davidson (CSIRO Process Science and Engineering) for preparation of samples for SEM and EPMA.

REFERENCES

1) L.-H. Hsieh and J. A. Whiteman: *ISIJ Int.*, **29** (1989), 24.
2) L.-H. Hsieh and J. A. Whiteman: *ISIJ Int.*, **29** (1989), 625.
3) Y. Hida, M. Sasaki, K. Sato, M. Kagawa, M. Takeshi, H. Soma, H. Naito and M. Taniguchi: *Nippon Steel Tech. Rep.*, **35** (1987), 59.
4) Y. Hida, J. Okazaki, K. Itoh and M. Sasaki: *Tetsu-To-Hagané*, **73** (1987), 1893.
5) F. Matsuno: *Trans. Iron Steel Inst. Jpn.*, **19** (1979), 595.
6) F. Matsuno and T. Harada: *Trans. Iron Steel Inst. Jpn.*, **21** (1981), 318.
7) N. V. Y. Scarlett, M. I. Pownceby, I. C. Madsen and A. Christensen: *Metall. Mater. Trans. B*, **35** (2004), 929.
8) N. V. Y. Scarlett, I. C. Madsen, M. I. Pownceby and A. N. Christensen: *J. Appl. Crystallogr.*, **37** (2004), 362.
9) N. A. S. Webster, M. I. Pownceby, I. C. Madsen and J. A. Kimpton: *Metall. Mater. Trans. B*, **43** (2012), 1344.
10) N. A. S. Webster, M. I. Pownceby, I. C. Madsen and J. A. Kimpton: *ISIJ Int.*, **53** (2013), 774.
11) W. G. Mumme, J. M. F. Clout and R. W. Gable: *Neues Jahrb. Miner. Abh.,* **173** (1998), 93.
12) J. McAndrew and J. M. F. Clout: Proc. of 4th China-Australia Symp. on the Technology of Feed Preparation for Ironmaking, Dampier, Australia, (1993), 1.
13) J. Hancart, V. Leroy and A. Bragard: *C.N.R.M. Report*, DS 24/67 (1967), 3.
14) S. N. Ashan, T. Mukherjee and J. A. Whiteman: *Ironmaking Steelmaking*, **10** (1983), 54.
15) T. R. C. Patrick and M. I. Pownceby: *Metall. Mater. Trans. B*, **32** (2001), 1.
16) TOPAS Version 4.2, Bruker AXS Inc., Madison, Wisconsin, USA, (2009).
17) R. Blake, R. Hessevick, T. Zoltai and L. Finger: *Am. Mineral.*, **51** (1966), 123.
18) E. N. Maslen, V. A. Strel'tsov, N. R. Strel'tsova and N. Ishizawa: *Acta Crystallogr.*, **B51** (1995), 929.
19) H. Saalfeld and M. Wedde: *Z. Krystallogr. Krist.*, **139** (1974), 129.
20) G. A. Lager, J. D. Jorgensen and F. J. Rotella: *J. Appl. Phys.*, **53** (1982), 6751.
21) I. Oftedal: *Z. Phys. Chem.*, **128** (1927), 135.
22) P. Berastegui, S.-G. Eriksson and S. Hull: *Mater. Res. Bull.*, **34** (1999), 303.
23) D. F. Decker and J. S. Kasper: *Acta Crystallogr.*, **10** (1957), 332.
24) A. V. Arakcheeva and O. G. Karpinskii: *Sov. Phys. Crystallogr.*, **32** (1987), 31.
25) W. C. Hamilton: *Phys. Rev.*, **110** (1958), 1050.
26) I. C. Madsen, I. E. Grey and S. Mills: *Mater. Sci. Forum*, **651** (2010), 37.
27) R. J. Hill and C. J. Howard: *J. Appl. Crystallogr.*, **20** (1987), 467.
28) I. C. Madsen and N. V. Y. Scarlett: Powder Diffraction: Theory and Practice, ed. by R. E. Dinnebier and S. J. L. Billinge, The Royal Society of Chemistry, Cambridge, (2008), 298.
29) K. Kihara: *Eur. J. Mineral.*, **2** (1990), 63.
30) M. I. Pownceby and J. M. F. Clout: *T. I. Min. Metall. C*, **109** (2000), 36.
31) J. S. Huebner: Research Techniques for High Temperature and High Pressure, ed. by G. C. Ulmer, Springer-Verlag, New York, (1971), 123.